ORIGINAL SCIENTIFIC PAPER

CROATICA CHEMICA ACTA

Croat. Chem. Acta **2024**, *97*(4), 275–283
Published online: June 21, 2025, 275–283
DOI: 10.5562/cca4143

HKD 1926

A Simple Method for Evaluating Photochemical Dependencies in the Atmosphere

Katja Džepina,[1,2,3] Sasha Madronich,[1,*]

[1] National Center for Atmospheric Research, Atmospheric Chemistry Division, 1850 Table Mesa Drive, PO Box 3000, Boulder, CO 80305, USA

[2] Ruđer Bošković Institute, Physical Chemistry Division, Laboratory for Chemical Kinetics and Atmospheric Chemistry, Bijenička cesta 54, 10002 Zagreb, Croatia

[3] PSI Center for Energy and Environmental Sciences, 5232 Villigen PSI, Switzerland

* Corresponding author's e-mail address: sasha@ucar.edu

RECEIVED: November 25, 2024 * REVISED: April 4, 2025 * ACCEPTED: April 15, 2025

THIS PAPER IS DEDICATED TO THE LATE PROFESSORS TOMISLAV CVITAŠ AND LEO KLASINC

Abstract: This work examines the photochemistry of the lower troposphere for clean high latitudes in spring 2000 during the Tropospheric Ozone Production about the Spring Equinox (TOPSE) experiment. TOPSE measurements included the short-lived quantities [OH], [HO_2] + [RO_2], and [NO]/[NO_2] as well as those slow varying ones that, according to photo-chemical theory, control them, e.g. [H_2O], [O_3], [NO_x], [CO], temperature T, pressure p, and photolysis rate coefficients (*J*-values). We examine this control using a simple scaling equation, which we term local sensitivity function (LSF), to correlate simultaneous measurements:

$$[X] \propto [H_2O]^{\alpha}[O_3]^{\beta}[NO_x]^{\gamma}[CO]^{\delta}[J]^{\varepsilon}[T]^{\varphi}[p]^{\chi}$$

where X = OH, HO_2 + RO_2, or NO/NO_2 ratio, and the exponents α, β, γ, δ, ε, ϕ, and χ are estimated with box model. We first test this correlation using the output from a regional chemistry-transport model (CTM) and find a remarkable improvement in the correlation between X and the LSF, compared to correlations of X with any single parameter (e.g., *J* values). When using actual observations, the correlations for OH remain unchanged, those for HO_2 + RO_2 improve significantly, but the correlation of the observed NO/NO_2 ratio with its LSF is sharply worse than simple correlations (e.g. vs. *J* value). This surprising result suggests that neither the box model nor the CTM are representing the chemistry of NO and NO_2 correctly in the polar troposphere, and points to the importance of other reactions, e.g., BrO + NO → Br + NO_2 and aerosol heterogeneous chemistry ones, that are not currently in the models.

Keywords: TOPSE experiment, polar troposphere, photochemistry, box model Master Mechanism, chemistry-transport model HANK.

INTRODUCTION

THE photochemistry of the troposphere links many time scales, from microseconds to decades. These links are inherent in bimolecular reactions, e.g. for the reaction of hydroxyl radicals (OH) with carbon monoxide (CO) with rate constant k,

$$OH + CO\ (+O_2) \rightarrow HO_2 + CO_2 \qquad (1)$$

where one can define two complementary lifetimes, τ_{OH}^{-1} = k[CO] and τ_{CO}^{-1} = k[OH]. Typically, τ_{OH} ~ 1 s while τ_{CO} ~ several weeks, so that short-term fluctuations in OH are controlled by CO (among other factors), but the life-times and concentrations of CO are controlled largely by time-integrated OH. While much of the interest in atmospheric chemistry focuses on large-scale (temporal or spatial) impacts, it is equally necessary to understand the local and instantaneous behaviors because precisely the same processes may be involved.

The Tropospheric Ozone Production about the Spring Equinox 2000 (TOPSE) experiment, with its airborne measurements of key radicals and their controlling chemical and physical factors, generated a rich data set for testing known photochemical theory. In this work, we consider a subset selected for studying the response of short-lived species to changes in longer-lived species and photolytic radiation. Specifically, we examined the concentration of hydroxyl radicals [OH], the total concentration of peroxy radicals (sum of hydro-peroxy [HO_2] and organic peroxy [RO_2] radicals, [HO_2] + [RO_2]) and

the ratio of nitric oxide to nitrogen dioxide [NO]/[NO_2]. The production and destruction rates of these radicals, as well as the NO–NO_2 partitioning, should be mostly in balance on short time scales, while tracking the slower changes in local physical and chemical conditions. In practice, such environmental drivers include photolytic radiation ($h\nu$), temperature (T), water (H_2O), ozone (O_3), carbon monoxide (CO), nitrogen oxides (NO_x = NO + NO_2), and volatile organic carbon species (VOCs, including methane (CH_4), non-methane hydrocarbons (NMHCs), and hetero-substituted organics).[1–3] Many of these quantities were measured simultaneously during TOPSE.

Analytic expressions that describe how these radicals depend on longer-lived species are difficult to derive even with steady state approximations, and in practice numerical solution methods are employed.[4] Simple empirical correlations, e.g. between OH and NO_x concentrations, are usually poor and difficult to interpret because of the simultaneous and more or less independent changes in the other driving factors (e.g. ambient concentrations of H_2O, O_3, and CO).

Here, we propose a simple expression, which we term the local sensitivity function (LSF), to capture the simultaneous variations in the aforementioned driving factors of photochemistry:

$$[X] \propto [H_2O]^{\alpha} [O_3]^{\beta} [NO_X]^{\gamma} [CO]^{\delta} [J]^{\varepsilon} [T]^{\varphi} [p]^{\chi} \quad (1)$$

where ambient concentrations of X = OH, HO_2 + RO_2, or NO/NO_2 are measured during TOPSE, as are those of H_2O, O_3, NO_x, CO, and values of J, temperature (T), and pressure (p). The exponents α, β, γ, δ, ε, ϕ, and χ are estimated for each measured parameter by sensitivity studies with a photo-chemical box model. To the extent that the TOPSE measurements can be correlated in this way, it could be argued that local photochemistry is understood at least as to the relative importance of these controlling variables. On the other hand, the lack of such correlation, or any significant deviations from it (e.g., in linearity and zero intercept), could be due to instrumental scatter and possible artifacts, but also to important processes (e.g., heterogeneous chemistry) and quantities (e.g., other gas-phase species) that are not considered in our model.

MEASUREMENTS AND MODELS

Measurements of Chemical Species and Meteorological Parameters

Perhaps the simplest chemical regime to study and validate the understanding of atmospheric photochemical processes is under the clean background conditions found in the remote free troposphere. The aircraft-based TOPSE measurements used in initializing the box model simulations in this work are shown in Table 1, with detailed descriptions of the analytical techniques used in measurement in the references listed in Table 1. To select a representative TOPSE data set for clean background conditions we used the following filtering criteria: 1) aircraft measurements altitude between 1 and 6 km (where most of OH data is available), 2) latitude between 55°N and 85°N, 3) NO mixing ratio less than 20 pptv, 4) CO mixing ratio less than 150 ppbv, 5) n-butane mixing ratio less than 175 pptv, and 6) availability of OH data. These selection criteria were used to filter out the direct influence of stratospheric air intrusions and local surface emissions. Table 2 lists basic statistics for the data points thus selected. Measurements below detection limit were set at half the detection limit for the purpose of averaging. This filtered ambient data set is characterized by cold temperatures (median 243 K), low water vapor (median 0.96 g kg^{-1}) and low NO_x conditions (median 23 pptv). Photolysis frequencies are highly variable depending on the time and location of the measurement, with maximum and minimum $J(O_3)$ for reaction $O_3 + h\nu \rightarrow O_2 + O(^1D)$ of 3.3×10^{-5} sec^{-1} and 1.3×10^{-6} sec^{-1}, respectively. Nighttime measurements were not used.

Table 1. TOPSE measurements.

Measurment	Technique	Principal Investigator	Reference[a]
O_3	Chemiluminescence	B. Ridley	[5]
NO	Chemiluminescence	B. Ridley	[5]
NO_2	NO_2 Photolysis / Chemiluminescence	B. Ridley	[5]
PAN, PPN	Gas Chromatography / Electron Capture Detector	F. Flocke	[6]
HNO_3	Mist Chamber / Ion Chromatography	R. Talbot	[7]
H_2O_2, CH_3COOH	High Performance Liquid Chromatography	B. Heikes	[8]
HCHO	Tunable Diode Laser	A. Fried	[9]
CO	Tunable Diode Laser	M. Coffey	[b]
NMHCs	Canister Sampling/ Gas Chromatography	D. Blake	[10]
H_2O	Tunable Diode Laser	B. Gandrud	[11]
OH	Chemical Ionization Mass Spectrometry	F. Eisele	[12]
RO_2	Chemical Ionization Mass Spectrometry	C. Cantrell	[13]
Photolysis rate	Scanning Spectroradiometer	R. Shetter	[14]

(a) [5] Ridley et al., 1996; [6] Flocke et al., 2005; [7] Talbot et al., 1999; [8] Lee et al., 1995; [9] Fried et al., 1998; (b) M. Coffey, *pers. comm.*; [10] Blake et al., 1997; [11] Jensen et al., 2001; [12] Tanner et al., 1997; [13] Cantrell et al., 2003; [14] Shetter et al., 1999.

Table 2. Selected background conditions.[a]

Variable	Mean ± St dev	Median	Maximum	Minimum
Latitude / °	70 ± 8	73	85	55
Longitude / °	–80 ± 10	–81	–53	–97
Altitude / m	4400 ± 1500	5200	5997	1004
Pressure / mbar	570 ± 130	510	892	443
Temperature / K	245 ± 11	243	272	228
Julian day / days	63 ± 10	64	81	40
Water vapor / g kg^{-1}	0.49 ± 0.67	0.22	3.70	0.01
GOME O_3 / DU	360 ± 30	356	480	295
O_3 / ppbv	68 ± 14	66	125	33
NO / pptv	10 ± 5	10	20	DL
NO_2 / pptv	13 ± 8	12	39	DL
NO_x / ppzv	23 ± 11	23	55	1
NO_y / pptv	340 ± 102	338	671	106
PAN / pptv	248 ± 83	238	464	89
PPN / pptv	36 ± 12	36	79	11
HNO_3 / pptv	68 ± 48	62	383	4
HCHO / pptv	76 ± 63	70	311	DL
H_2O_2 / pptv	194 ± 132	174	1550	DL
CH_3OOH / pptv	157 ± 93	144	588	DL
CO / ppbv	143 ± 6	145	150	119
CH_4 / ppmv	1.83 ± 0.01	1.83	1.87	1.79
Ethane / pptv	1490 ± 250	1400	2386	958
Propane / pptv	310 ± 190	210	974	115
n-Butane	61 ± 62	29	284	6
n-Pentane	9 ± 12	4	67	DL
Benzene / pptv	55 ± 32	38	188	21
Ethyne / pptv	304 ± 117	242	838	180
i-Pentane / pptv	11 ± 5	3	78	DL

(a) Median values from the above table were chosen to initialize model for altitude range of 1–6 km, high latitudes of 55-85°N and values of NO < 20 pptv and CO < 150 ppbv, with the following addition: $[H_2]$ = 600 ppbv.

The above selection procedure yielded 859 sets of simultaneously observed concentrations and conditions (i.e., data points). These points were then used in two distinct ways: 1) their median values were used as initial conditions for box model simulations (described in Sections 3.1 and 3.2); and 2) the individually measured concentrations were used to develop correlations with the LSF (described in Section 3.3). For this second purpose, the selection of individual points was further narrowed as follows: a) for correlations involving OH, we used only points from the last two TOPSE missions (6 and 7) for which the accuracy has been established (F. Eisele, pers. comm.) (112 points remaining); b) for the correlations with HO_2 + RO_2, points with missing HO_2 + RO_2 were excluded (494 points remaining); and c) for correlations with NO/NO_2 ratio, we only used data with NO values at least five times above the detection limit and NO_2 values at least twice the detection limit (111 points remaining).

The Approximation of Linear Superposition in log-log Space

A short-lived quantity X (where X = OH, HO_2 + RO_2, or NO/NO_2) is typically a complex function of several long-lived parameters Y_i (where Y_i = *J*, O_3, H_2O, NO_x, CO, T, and p). Here we approximate its local response near X_0, $Y_{i,0}$ by a linear superposition of independent logarithmic terms:

$$ln\frac{x}{x_o} \approx \sum \alpha_i \, ln\frac{Y_i}{Y_{i,0}} \quad (2)$$

where higher order and cross terms are ignored. The coefficients α_i represent the slopes in the $\ln Y_i$ direction of the plane tangent to the lnX surface near $\ln X_0$, $\ln Y_{i,0}$, and are constant in the sense that they don't depend on any of the driving variables $Y_{i,0}$. Exponentiating both sides of Eq. 2 leads to the working Eq. 1, after identifying and assigning X for the short-lived quantities and Y_i for the long-lived drivers.

We posit that the superposition in Eq. 1 should explain more of the X / X_0 variance than any individual parameter Y_i / $Y_{i,0}$. The coefficients α_i can be estimated from a chemical kinetic model representing the main chemical processes thought to be occurring for the TOPSE conditions. The next section describes the chemical kinetic model which was used to estimate the coefficients α_i.

Description of the Box Model

The 0-dimensional (or box) model used in this study is the NCAR Master Mechanisms[15–16] with updates.[17] Inorganic reactions were updated with the recommendations of DeMore et al.[18] Additional updates to the kinetic data since 2000 are relatively minor and do not affect our main results. The hydrocarbon chemistry is treated explicitly and includes the photo-oxidation of intermediate partly oxygenated organics. Alkanes up to C8, alkenes up to C4, aromatics up to C8 and two biogenic compounds, isoprene and α-pinene, are considered as initial hydrocarbons reagents in the gas-phase mechanism. Integrations were carried out for five simulation days, starting at midnight, with constant temperature and pressure and the full diurnal light cycle. Photolysis rate coefficients were calculated using the Tropospheric Ultraviolet Visible (TUV) radiative transfer model[19,20] for one day at 15 min increments and then duplicated for the remaining four days.

The photo-chemical budgets for OH, RO_x and O_x were simulated over a 5 day cycle under the selected pristine conditions (described in Section 2.1). Photolysis frequencies were calculated for May 22, 2000 (which corresponds to TOPSE Mission 7 dated May 15–23, 2000) using an O_3 column = 356 DU, latitude and altitude from Table 2, and an assumed snow surface albedo = 0.75. The model was initialized with the measured median temperature, pressure and chemical species mixing ratios. The simulations were made with constant CO, CH_4, NMHCs, HCHO, O_3, PAN, PPN, HNO_3, H_2O_2 and CH_3OOH so that short-lived species (OH, HO_2, RO_2) could approach steady state, using the measured median mixing ratios of the longer-lived gases. NO_x was also held constant throughout the simulations. However, the NO/NO_2 ratio was allowed to vary. A Gear solver was used to calculate all remaining time-dependent concentrations, reaction rates, and various budgets (e.g. O_x, NO_x, HO_x) used in the discussion of the results.

The box model was used for the calculation of the exponents of the LSF, which are essentially normalized sensitivity coefficients calculated here as:

$$\alpha = \frac{\ln\frac{X}{X_0}}{\ln\frac{Y}{Y_0}} \quad (3)$$

The coefficients give the response of a short-lived quantity X = [OH], $[HO_2]$ + $[RO_2]$, or the ratio $[NO]/[NO_2]$, to changes in Y = photolysis coefficients, *J*, temperature T, and longer-lived species $[H_2O]$, $[O_3]$, [CO], and $[NO_x]$. We examined these changes relative to a reasonably representative central state x_0, y_0. Again, we used mostly the median values from Table 2 to initialize the model, with however constant CO, H_2O, O_3, NO_x, HCHO, H_2O_2 and CH_3OOH. *J* values were calculated for May 22, 2000 using O_3 column = 356 DU, latitude = 55˚N, altitude = 2 km, and surface albedo = 0.75.

This simulation served as the reference, or central point (X_0, Y_0) in Eq. 3. Then $[H_2O]$, $[O_3]$, [CO], $[NO_x]$, *J*, T, and p were changed, one at the time, by factors of 2 (factor of 4 range), ±10K for T and ±100 mbar for p. The results at noon of the third day were then compared with the reference run to calculate the sensitivity coefficients using

Table 3. Model sensitivity coefficients (×100) for background conditions.

	OH	HO_2	RO_2	$HO_2 + RO_2$	NO/NO_2
H_2O	33 ± 5[(a)]	25 ± 3	33 ± 5	26 ± 3	–5 ± 1
O_3	29 ± 13	19 ± 1	67 ± 14	26 ± 4	–82 ± 5
NO_x	15 ± 4	0 ± 0	–12 ± 3	–2 ± 1	–1 ± 0
CO	–58 ± 8	16 ± 2	–67 ± 6	4 ± 1	0 ± 0
J[(b)]	107 ± 6	54 ± 1	31 ± 2	51 ± 1	89 ± 2
T	237 ± 67	191 ± 11	637 ± 51	253 ± 7	–525 ± 6
p	–56 ± 0	–36 ± 0	48 ± 1	–37 ± 0	7 ± 1

(a) Error estimates are range of variation when doubling or halving the central values of H_2O, O_3, NO_x, CO, or *J*; ± 10K and ± 100 mbar in the cases of T and p, resp.
(b) Photolysis coefficient for $O_3 \rightarrow O_2 + O(^1D)$ is used in radical correlations, and for $NO_2 \rightarrow NO + O(^3P)$ in NO/NO_2 correlations.

Eq. 3. These coefficients are summarized in Table 3 and their physical interpretations are discussed in Section 3.2. We note that, because a simple power relation (Eq. 3) cannot capture the complexity of the full chemical system, slightly different coefficients were obtained depending on whether an independent variable Y was increased or decreased relative to Y_0. The average of these two values is given in Table 3, while half of their difference is given as an estimate of the associated error.

RESULTS AND DISCUSSION

Photo-chemical Budget

Box model simulations of gas-phase chemical species in the pristine atmosphere conditions were performed to gain an understanding of behavior of species studied in this work. Diurnal evolutions and budgets of key gas-phase species HO, RO_x (OH + HO_2 + RO_2) and O_x (O_3 + NO_2) computed by box model are shown in Figure 1. The budgets are shown for the fifth day of the simulation so as to give other non-fixed intermediates enough time to reach near steady state conditions.

Detailed description of modeled mechanism for production and loss of radical species is given in Supplementary Information section (SI Section S1). Briefly, the budget analysis shows that a few parameters and long-lived chemicals play a critical role in controlling the fast radical photochemistry. These include CO, CH_4, H_2O, NO_x, O_3 and photolysis frequencies. Since CH_4 variability is minimal, its variability will not play a critical role in short-term fluctuations in measured levels of radicals (OH and HO_2 + RO_2) and NO/NO_2 ratio. However CO, H_2O, NO_x, O_3 and photolysis frequencies can be quite variable in space and time and thus should be considered as important controls on radical photochemistry. Note that direct evaluation of the modeled HO_x, RO_x, and O_x budgets with observations is difficult because production and loss rates are not measured directly. We note that the small net production of O_x is consistent with the observation that O_3 concentrations were relatively steady during TOPSE.[21]

Sensitivity Coefficients

The model-calculated sensitivity coefficients, given in Table 3, are mainly less than unity, can be negative, and have fairly small ranges (shown as errors in Table 3) even over the large variations explored. The detailed sensitivities depend on the complexity of the entire chemical system, but some major features can be understood easily.

The primary production of OH occurs from the ozone photolysis reaction (R1):

$$O_3 + h\nu \rightarrow O_2 + O(^1D)(+H_2O) \rightarrow O_2 + 2\ OH \qquad (R1)$$

hence OH is expected to scale approximately linearly with the photolysis coefficient $J(O_3)$ (sensitivity coefficient of 1.07 in Table 3). The formation of OH initiates the HO_x cycle (HO_x = OH + HO_2) via the reactions (R2–3):

$$OH + CO(+O_2) \rightarrow HO_2 + CO_2 \qquad (R2)$$

$$HO_2 + NO \rightarrow OH + NO_2 \qquad (R3)$$

The main loss of HO_x is the production of hydrogen peroxide (R4):

$$HO_2 + HO_2 \rightarrow H_2O_2 + O_2 \qquad (R4)$$

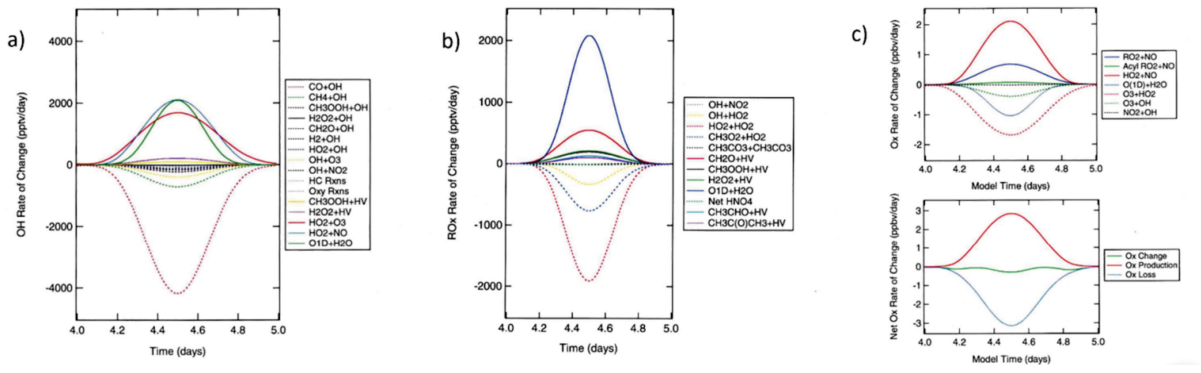

Figure 1. Gas phase reaction rates for the selected TOPSE conditions (Table 2), calculated with a box model. Panels show the major reactions affecting: (a) OH; (b) RO_x (RO_x = OH + HO_2 + RO_2); and (c) O_x (O_x = O_3 + NO_2). Legends in Figure 1 panels use the following notation: HV is the photon in photolysis reactions (Figs. 1a–1b); HC and Oxy Rxns are non-methane hydrocarbons and oxygenated organic intermediates reactions (Fig. 1a); Net HNO_4 is the total reactivity of RO_x with Peroxynitric acid, HNO_4 (Fig. 1b); and Acyl RO_2 are acyl peroxy radicals (Fig. 1c).

Steady state HO_x levels are determined by the balance between formation and loss (R1 vs. R4), the latter being quadratic in HO_2, thus steady state HO_2 concentrations are expected to scale with the square root of the primary production rate (see Ridley et al.[22] for a full discussion), consistent with the sensitivity exponent of 0.54 (Table 3) found from the box model.

Concentrations of OH and HO_2 are not sensitive to NO_x (small exponents in Table 3) since NO_x affects the OH/HO_2 partitioning via reaction R3, but not the total HO_x levels. Carbon monoxide tends to decrease OH via reaction R2 (negative sensitivity coefficient, –0.58, Table 3), but the effect on HO_2 is more complex due to the competition with CH_4 for OH.

The NO/NO_2 ratio in both the box model and the chemistry-transport model (CTM) is controlled mostly by the reactions (R3, R5–R6):

$$NO_2 + h\nu\,(+O_2) \rightarrow NO + O_3 \qquad \text{(R5)}$$

$$NO + O_3 \rightarrow NO_2 + O_2 \qquad \text{(R6)}$$

$$NO + HO_2 \rightarrow NO_2 + OH \qquad \text{(R3)}$$

Thus the NO/NO_2 ratio is expected to be insensitive to CO, H_2O, and NO_x (as also seen in Table 3) and depends mainly on $J(NO_2)$ (R5) and O_3 (R6). The strong dependence on T (sensitivity coefficient of –5.25 in Table 3) is noteworthy, and is due to the rate constant of reaction R6, which has a large activation energy of 12500 J mol^{-1}.[23] Detailed overview of the known photochemistry occurring in the pristine troposphere pertaining to LSFs sensitivity coefficients in this work is given in Supplementary Information (SI Section S2).

Photochemical Dependencies of Data Produced by Regional Model HANK

We applied the LSF methodology to the concentration fields of investigated species and quantities calculated for TOPSE conditions by a regional CTM HANK.[24] The model output is by definition free of instrumental scatter, and stems entirely from known processes and chemical mechanisms that are included in the model. The results are shown in Figure 2. HANK model results already show good correlations between OH and $HO_2 + RO_2$ vs. $J(O_3)$, and NO/NO_2 vs. $J(NO_2)$ (left panels of Figure 2), yet in all cases the correlations are significantly improved when using the LSF (right panels of Figure 2). The improvement for the NO/NO_2 ratio implies that the variability of this ratio is quantitatively ascribed to the variability of the LSF, which is dominated by T, O_3, and $J(NO_2)$ (see Table 3).

The success of our simple LSF-based correlation applied to HANK regional mode output indicates that both

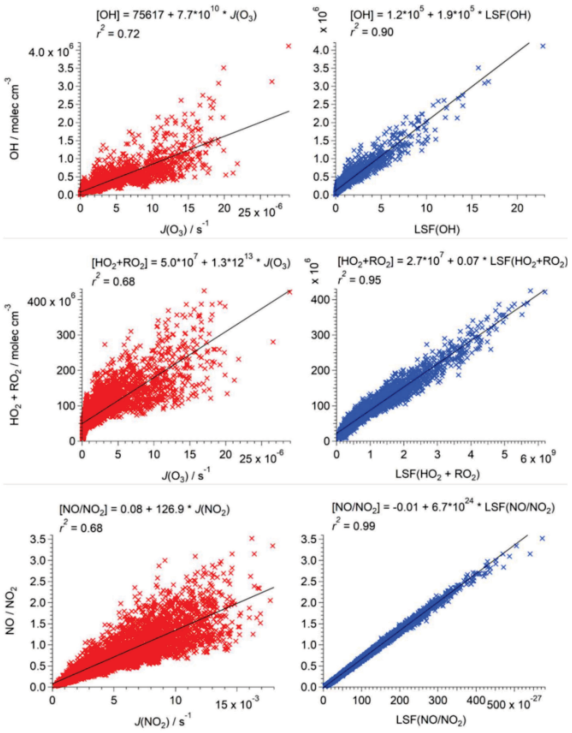

Figure 2. Correlations for the concentration fields during TOPSE campaign for modeled values calculated by a regional model. Left panels show correlations of modelled HANK results with J values, specifically OH and $HO_2 + RO_2$ vs. $J(O_3)$ in top two left panels ($O_3 + h\nu \rightarrow O_2 + O(^1D)$) and NO/NO_2 ration vs. $J(NO_2)$ in bottom most left panel ($NO_2 + h\nu \rightarrow NO + O(^3P)$). Right panels show correlations of modeled HANK results applied in the local sensitivity function (LSF, using the same exponents as for measured results, see Table 3 and Figure 3 caption), specifically: [OH] vs. $LSF(OH) = H_2O^{0.33}\, O_3^{0.29}\, NO_x^{0.15}\, CO^{-0.58}\, J(O_3)^{1.07}\, T^{2.37}\, p^{-0.56}$ (top right panel); $[HO_2 + RO_2]$ vs. $LSF(HO_2 + RO_2) = H_2O^{0.26}\, O_3^{0.26}\, NO_x^{-0.02}\, CO^{0.04}\, J(O_3)^{0.51}\, T^{2.53}\, p^{-0.37}$ (middle right panel); and $[NO]/[NO_2]$ vs. $LSF(NO/NO_2) = H_2O^{-0.05}\, O_3^{-0.82}\, NO_x^{-0.01}\, CO^{0.00}\, J(NO_2)^{0.89}\, T^{-5.25}\, p^{0.07}$ (bottom right panel).

the box model and regional CTM (HANK) have similar photochemical drivers, despite many differences in details of the chemistry, and the complex role of transport in the 3d HANK model. Obviously such details have not degraded the excellent correlations for the model results, so it is natural to ask if this remains true with actual observations.

Photochemical Dependencies of TOPSE Observations

The sensitivity coefficients given in Table 3 show that photolysis rate coefficients are the most important factors affecting OH, $HO_2 + RO_2$ and NO/NO_2 ratios. This is confirmed for the observations by direct correlations with

measured *J* values, shown by the left panels of Figure 3, and by the correlation coefficients summarized in Table 4. Other individual correlations shown in Table 4 and Figures S1–S3 (Supplementary Information section) are rather poor, and are in some cases opposite to simple expectations based on Table 3 (e.g., the negative correlation observed between HO_2 + RO_2 and CO). Such differences can arise because individual concentrations (e.g., of CO) may be correlated with other confounding factors (e.g., for stratospheric air, low CO would be typically associated with high O_3). The positive correlation of HO_2 + RO_2 with temperature (r^2 = 0.44) is not expected from our sensitivity analysis.

When the major driving factors of photochemistry are combined as part of the local sensitivity function LSF (Eq. 1), the correlations of species measured during TOPSE are expected to show less scatter, better linearity, and smaller intercepts. These new correlations are shown in the right panels of Figure 3, with their r^2 values also summarized in Table 4. The LSF correlation for OH shows a slight degradation, to r^2 = 0.56 from 0.58 vs. $J(O_3)$ alone (Figure 3 and Table 3). Its LSF includes contributions spread across many different factors (see Table 3), and if our sensitivity coefficient for any one of them were seriously in error, further degradation of r^2 would have been expected. It is likely that instrumental scatter of OH measurements which is significant, is limiting the correlation. For HO_2 + RO_2, the LSF provides a substantial improvement, with r^2 = 0.55, a value not reached by any individual correlation. As for OH, it is likely that instrumental scatter is an important part of the unexplained variance. The observed NO/NO_2 ratio correlates moderately with $J(NO_2)$ (r^2 = 0.49), but poorly with the LSF (which does contain $J(NO_2)$ among other factors). Instrumental scatter in the measurements of $J(NO_2)$ is already implicit in the direct correlation with $J(NO_2)$, and is clearly not the reason for the collapse of the correlation when the LSF is used. This result is even more surprising in view of the HANK results, for which the LSF led to near perfect correlation (r^2 = 0.998). The sharp contrast between these results indicates that something is fundamentally wrong in our models, be they box or 3d CTM.

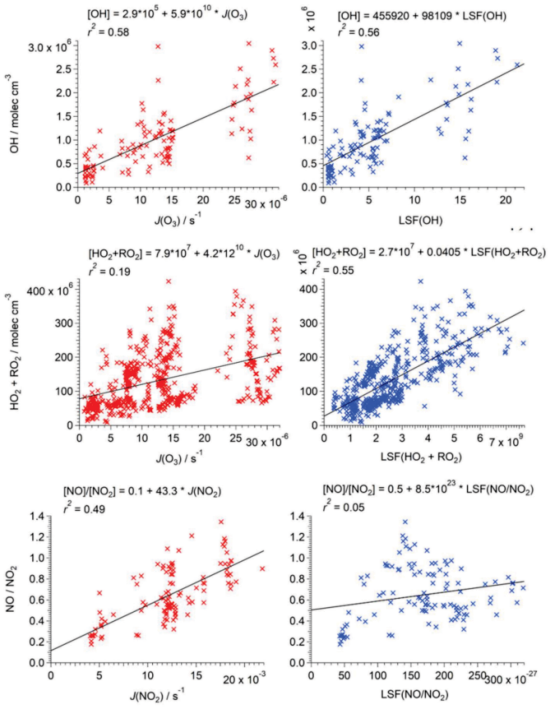

Figure 3. Correlations of OH, HO_2 + RO_2 and NO/NO_2 ratio measured during TOPSE. Left panels show correlations against measured *J* values, specifically OH and HO_2 + RO_2 vs. $J(O_3)$ in top two left panels (O_3 + $h\nu$ → O_2 + $O(^1D)$) and NO/NO_2 ration vs. $J(NO_2)$ in bottom most left panel (NO_2 + $h\nu$ → NO + $O(^3P)$). Right panels show correlations with the local sensitivity function (LSF, see text), specifically: [OH] vs. LSF(OH) = $H_2O^{0.33}$ $O_3^{0.29}$ $NO_x^{0.15}$ $CO^{-0.58}$ $J(O_3)^{1.07}$ $T^{2.37}$ $p^{-0.56}$ (top right panel); [HO_2 + RO_2] vs. LSF(HO_2 + RO_2) = $H_2O^{0.26}$ $O_3^{0.26}$ $NO_x^{-0.02}$ $CO^{0.04}$ $J(O_3)^{0.51}$ $T^{2.53}$ $p^{-0.37}$ (middle right panel); and [NO]/[NO_2] vs. LSF(NO/NO_2) = $H_2O^{-0.05}$ $O_3^{-0.82}$ $NO_x^{-0.01}$ $CO^{0.00}$ $J(NO_2)^{0.89}$ $T^{-5.25}$ $p^{0.07}$ (bottom right panel).

Table 4. Correlation coefficients (r^2) for selected TOPSE measurements at background conditions.

	OH	HO_2 + RO_2	NO/NO_2
H_2O	*0.01*[a]	**0.23**	*0.00*
O_3	0.07	0.00	0.07
NO_x	0.01	0.03	0.00
CO	*0.06*	**0.21**	0.00
J[b]	**0.58**	**0.19**	**0.49**
T	0.00	**0.45**	0.03
P	*0.00*	0.32	0.01
LSF[c]	**0.56**	0.55	0.05

(a) Italics indicate negative correlations. Bold font indicates values larger than 0.1.
(b) Photolysis coefficient used for OH and HO_2 + RO2 correlations is $J(O_3)$ (O_3 → O_2 + $O(^1D)$), and for NO/NO_2 ones is $J(NO_2)$ (NO_2 → NO + $O(^3P)$).
(c) Local sensitivity function, see text.

Examination of Table 3 shows that NO/NO_2 is expected to be sensitive not only to $J(NO_2)$, but also to O_3 and especially T. The sensitivity to T arises from the assumption that NO → NO_2 conversions are dominated by reaction R6 which, as mentioned above, has a very large activation energy. If this is wrong, i.e., if a different less T-sensitive reaction is the main cause of NO → NO_2 conversions, then our application of the LSF with the overestimated sensitivity to T might indeed be expected to degrade the correlation.

One possibility is the rapid reaction of bromine oxide (R7):

$$BrO + NO \rightarrow Br + NO_2 \quad (R7)$$

Using rate constants for reactions R6 and R7 of k(R6) = 3×10^{-12} exp (–1500/T) and k(R7) = 8.8×10^{-12} exp(260/T), both in the units of cm^3 $molec^{-1}$ s^{-1}, and median O_3 (66 ppb) and T (243 K) from Table 2, we estimate that the two reaction rates become comparable for BrO concentrations of approx. 15 ppt. Measurements of BrO were not available during TOPSE, but Volkamer et al.[23] found concentrations of 3 ppt or lower, suggesting at best only a partial role for reaction R7. Other processes missing in the models, e.g., heterogeneous chemistry on the surface of aerosols, may be determining the NO/NO_2 ratios. Our simple analysis clearly shows that, whatever the answer, the chemistry of the polar troposphere is not fully understood.

While the improvements in correlations using the LSF for OH and HO_2 + RO_2 are modest compared to using *J* values only, their significance should not be underestimated. Each of the additional factors in the LSF (H_2O, O_3, CO, NO_x, T, and p) is itself highly variable within the selected data set (e.g., see range of values in Table 2), and its inclusion could potentially worsen rather than improve the correlation. When we purposely randomized the H_2O, O_3, CO, NO_x, T, and p data (so that simultaneously measured data points were no longer co-associated), we indeed found that correlations degraded sharply compared to those using *J* values alone. Only the use of simultaneously measured values led to improved correlations.

We also examined correlations with the same functional form (LSF, Eq. 1), but this time estimating the sensitivity exponents (α–χ) using a least squares optimization procedure, rather than deriving them from the box model simulations. Although the values of the exponents were in some cases significantly different than the model-derived ones, improvements in r^2 were only minor. This lack of improvement suggests that the physically-based sensitivity coefficients (i.e., those derived from the chemical model) do indeed capture much of the photochemically driven variability within the data set, and are therefore more applicable to clean tropospheric conditions in general than sensitivities derived with a purely empirical fitting approach.

CONCLUSIONS

We used a simple semiempirical parameterization (the LSF) to correlate photochemically relevant species measured during the TOPSE field campaign. Some of these correlations were in agreement with the expectation from box and 3d models, but not for the NO/NO_2 ratio which appears to be controlled by factors not in the current models.

The methodology developed here is generally applicable when evaluating correlations among species having very different lifetimes. The sensitivity coefficients are essentially a generalization of the notion of reaction order in chemical kinetics, extended to include also dependence on environmental factors such as T, p, and *J* values. Accurate calculation of these sensitivities and their validation with observations, such as attempted here, are critical to demonstrate predictive ability in atmospheric chemistry.

Acknowledgment. We are grateful to Craig Stroud for producing the box model simulations of photochemical budgets and to Peter Hess for simulations with the regional model HANK. We also extend our gratefulness to the team members of the TOPSE experiment for proving us with their measurements datasets used in this work: J. Zheng, Eliot Atlas, Don Blake, Chris Cantrell, Mike Coffey, Fred Eisele, Frank Flocke, Alan Fried, Lee Mauldin, Bryan Wert, Bruce Gandrud, Brian Heikes, Brian Ridley, Richard Shetter, and Bob Talbot. Finally, this work is dedicated to the loving memory of Leo Klasinc and Tomislav Cvitaš, our friends, mentors and role models.

Supplementary Information. Supporting information to the paper is attached to the electronic version of the article at: https://doi.org/10.5562/cca4143.

PDF files with attached documents are best viewed with Adobe Acrobat Reader which is free and can be downloaded from Adobe's web site.

REFERENCES

[1] P. A. Leighton, *Photochemistry of Air Pollution*, Academic Press, New York, **1961**.

[2] J. H. Seinfeld, S. N. Pandis, *Atmospheric Chemistry and Physics: From Air Pollution to Climate Change*, John Wiley and Sons, Inc., New York, **1997**.

[3] B. J. Finlayson-Pitts, J. N. Pitts, Jr., *Chemistry of the Lower and Upper Atmosphere*, Academic Press, San Diego, **2000**.

[4] G. P. Brasseur, D. J. Jacob, *Modeling of Atmospheric Chemistry*, Cambridge University Press, **2017**, 567. https://doi.org/10.1017/9781316544754

[5] B. A. Ridley, J. E. Dye, J. G. Walega, J. Zheng, F. E. Grahek, W. Rison, *J. Geophys. Res.* **1996**, *101*, 985–1000. https://doi.org/10.1029/96JD01706

[6] F. M. Flocke, A. J. Weinheimer, A. L. Swanson, J. M. Roberts, R. Schmitt, S. Shertz, *J. Atmos. Chem.* **2005**, *52*, 19–43. https://doi.org/10.1007/s10874-005-6772-0

[7] R. W. Talbot, J. E. Dibb, E. M. Scheuer, D. R. Blake, N. J. Blake, G. L. Gregory, G. W. Sachse, J. D. Bradshaw, S. T. Sandholm, H. B. Singh, *J. Geophys. Res.* **1999**, *104*, 5623–5638. https://doi.org/10.1029/98JD00879

[8] M. Lee, D. O'Sullivan, K. B. Noone, B. G. Heikes, *J. Atmos. Oceanic Technol.* **1995**, *12*, 1060–1072. https://doi.org/10.1175/1520-0426(1995)012<1060:MFTCAH>2.0.CO;2

[9] A. Fried, B. Henry, B. P. Wert, S. Sewell, J. R. Drummond, *Appl. Phys. B.* **1998**, *67*, 317–330. https://doi.org/10.1007/s003400050511

[10] N. J. Blake, D. R. Blake, T. Y. Chen, J. E. Collins, G. W. Sachse, B. E. Anderson, F. S. Rowland, *J. Geophys. Res.* **1997**, *102*, 28315–28325. https://doi.org/10.1029/97JD02538

[11] E. J. Jensen, O. B. Toon, S. A. Vay, J. Ovarlez, R. May, T. P. Bui, C. H. Twohy, B. W. N. Gandrud, R. F. Pueschel, U. Schumann, *J. Geophys. Res.* **2001**, *106*, 17253–17266. https://doi.org/10.1029/2000JD900526

[12] D. J. Tanner, A. Jefferson, F. L. Eisele, *J. Geophys. Res.* **1997**, *102*, 6415–6425. https://doi.org/10.1029/96JD03919

[13] C. A. Cantrell, G. D. Edwards, S. Stephens, L. Mauldin, E. Kosciuch, M. Zondlo, F. Eisele, *J. Geophys. Res.* **2003**, *108*, 8371–8384. https://doi.org/10.1029/2002JD002715

[14] R. E. Shetter, M. Muller, *J. Geophys. Res.* **1999**, *104*, 5647–5656. https://doi.org/10.1029/98JD01381

[15] S. Madronich, J. G. Calvert, *The NCAR Master Mechanism of the Gas-Phase Chemistry – Version 2.0*, Rep. NCAR-TN-333+STR, National Center for Atmospheric Research, Boulder, CO, **1989**.

[16] S. Madronich, J. G. Calvert, *J. Geophys. Res.* **1990**, *95*, 5697–5715. https://doi.org/10.1029/JD095iD05p05697

[17] B. Aumont, S. Madronich, I. Bey, G. S. Tyndall, *J. Atmos. Chem.* **2000**, *35*, 59–75. https://doi.org/10.1023/A:1006243509840

[18] W. B. DeMore, S. P. Sander, D. M. Golden, R. F. Hampson, M. J. Kurylo, C. J. Howard, A. R. Ravishankara, C. E. Kolb, M. J. Molina, *Chemical Kinetics and Photochemical Data for Use in Stratospheric Modeling, Evaluation 12*, JPL Publication 97-4, Jet Propulsion Laboratory, Pasadena, CA, **1997**.

[19] S. Madronich, S. Flocke, *Handbook of Environmental Chemistry (Ed.: P. Boule)*, Springer-Verlag, Heidelberg, **1998**, 1–26. https://doi.org/10.1007/978-3-540-69044-3_1

[20] S. Madronich, G. Weller, *J. Atmos. Chem.* **1990**, *10*, 289–300. https://doi.org/10.1007/BF00053864

[21] E. L. Atlas, B. A. Ridley, C. Cantrell, *J. Geophys. Res.* **2003**, *108*, 8353–8368. https://doi.org/10.1029/2002JD003172

[22] B. A. Ridley, S. Madronich, R. B. Chatfield, J. G. Walega, R. E. Shetter, M. A. Carroll, D. D. Montzka, *J. Geophys. Res.* **1992**, *97*, 10375–10394. https://doi.org/10.1029/91JD02287

[23] J. B. Burkholder, S. P. Sander, J. Abbatt, J. R. Barker, C. Cappa, J. D. Crounse, T. S. Dibble, R. E. Huie, C. E. Kolb, M. J. Kurylo, V. L. Orkin, C. J. Percival, D. M. Wilmouth, P. H. Wine, *Chemical Kinetics and Photochemical Data for Use in Atmospheric Studies, Evaluation No. 19*, JPL Publication 19-5, Jet Propulsion Laboratory, Pasadena, **2019**, 1–70.

[24] A. Klonecki, P. Hess, L. Emmons, L. Smith, J. Orlando, D. Blake, *J. Geophys. Res.* **2003**, *108*, 8367–8380. https://doi.org/10.1029/2002JD002199

[25] R. Volkamer, S. Baidar, T. L. Campos, S. Coburn, J. P. DiGangi, B. Dix, E. W. Eloranta, T. K. Koenig, B. Morley, I. Ortega, B. R. Pierce, M. Reeves, R. Sinreich, S. Wang, M. A. Zondlo, P. A. Romashkin, *Atmos. Meas. Tech.* **2015**, *8*, 2121–2142. https://doi.org/10.5194/amt-8-2121-2015